Experimental Evaluation of MIMO Radar Emissions From a Uniform Circular Array

Kyle S. Wanamaker, Matthew B. Heintzelman, Dan DePardo, Shannon D. Blunt, James M. Stiles
Radar Systems Lab, University of Kansas, Lawrence, KS

***Abstract* – Multiple-input multiple-output (MIMO) radar concepts exploit independently transmitted waveforms to generate spatially diverse emissions. In the context of uniform circular arrays (UCAs), an emergent phenomenon of linear phase progression around the array is orbital angular momentum (OAM), a topic that has experienced significant attention and has been purported to provide some benefits for radar. By extension, multi-modal OAM becomes a special case of MIMO. Herein we ask the question: what are the practical implications of simultaneously transmitting multiple OAM modes from a phased array, and how does this relate to more general MIMO radar concepts? Consequently, this work examines the far-field behavior of multi-modal OAM and an approximate version thereof involving a set of frequency modulated (FM) MIMO waveforms (obtained by constrained optimization), with the purpose of the latter being signals that can be generated at high-power. Relative performance is evaluated via Monte Carlo in simulation and through hardware implementation/assessment by open-air far-field experimentation.**

I. INTRODUCTION

In the collocated MIMO radar concept, each antenna element can transmit an independently generated waveform, thereby realizing spatial diversity that could be leveraged to enable enhanced resolution along the aperture extent [1] and/or improve discrimination by exploiting the multiplicative increase in degrees of freedom associated with coupling the fast-time and spatial domains [2]. Consequently, recent research has been directed toward optimizing MIMO waveforms to synthesize desired beampatterns [3] and producing prescribed array covariance matrices [4]. Of course, this increased dimensionality comes at the cost of self-induced cross-correlation interference, assuming the transmit waveforms coexist in time/space/frequency [5].

Uniform circular arrays (UCAs) have become a popular research topic due to their inherently broad spatial coverage and compact aperture. Additionally, when excited with a linear phase progression across the elements, the resulting beampatterns of such arrays may be decomposed into Bessel functions, resulting in cylindrically symmetric beams [6]. Such patterns could be advantageous in a surveillance context where it is desired to detect movers over a uniform azimuthal region. It has been shown that exciting a UCA with a linear phase progression also provides an efficient method for generating emissions carrying orbital angular momentum (OAM) [7]. With the spin momentum (polarization) of the electric field describing the orientation of the emissions' oscillations, OAM describes the tendency for the wavefront to twist about its propagation axis. Practical exploitation of OAM was first studied in the optical regime [8,9].

The synthesis of electromagnetic waves carrying OAM at radio frequencies (RF), first shown in 2007 [10], has recently gained attention for purported radar and communication applications due to the particular spatial properties that OAM can offer [11], including orthogonal modal decomposition [12,13]. Put another way, OAM possibly poses an alternative set of degrees of freedom, whereby orthogonal phase modes can be exploited to multiplex information when observed over a sufficiently large and coherent spatial aperture [14]. While most research into exploiting OAM for radar has focused on single-mode operation [15,16], multiplexing has also been examined in the context of linear arrays using specialized antennas [17]. The implementation of multi-modal OAM has been observed to be a form of multiple-input multiple-output (MIMO) operation [18].

Since standard multi-modal OAM emitted by a UCA would involve significant amplitude modulation (AM), thus effectively precluding amplifier operation in saturation, an FM MIMO emission structure is herein developed to approximate multi-modal OAM with waveforms that can be generated at high-power. This facilitates a comparison with MIMO waveforms designed according to traditional radar criteria (e.g. beamwidth and spectral containment) for which muti-modal OAM is an emergent phenomenon. To assess prospective radar utility these two related signal formats are evaluated via Monte Carlo simulation and employed for open-air experimentation on an X-band MIMO radar testbed.

II. SIGNAL MODEL

The far-field emission model of an aperture comprised of M antenna elements is directionally defined in azimuth ϕ (here expressed as the angle of rotation through the xy-plane) and elevation θ (measured off the positive z-axis). Under the far-field approximation, the radiated field pattern is modeled by the array factor

$$g(\theta,\phi) = \sum_{m=0}^{M-1} w_m e^{j\mathbf{k}^T\mathbf{p}_m} \tag{1}$$

where w_m denotes the complex amplitude weight for the mth transmit element and $\mathbf{p}_m \in \mathbb{R}^3$ is the position vector representing the corresponding spatial coordinates. For a UCA with elements lying in the xy-plane, the mth position vector is defined as

$$\mathbf{p_m} = \begin{bmatrix} x_m \\ y_m \\ z_m \end{bmatrix} = \begin{bmatrix} R_0 cos(\phi_m) \\ R_0 sin(\phi_m) \\ 0 \end{bmatrix}, \tag{2}$$

This work was supported by a subcontract with University of Missouri – Kansas City for research sponsored by the Defense Advanced Research Projects Agency under prime contract HR00112590137. DISTRIBUTION STATEMENT A. Approved for Public Release.

with R_0 the radius of the array and $\phi_m = \frac{2\pi m}{M}$ the azimuthal position of the mth element. The wavevector $\mathbf{k} \in \mathbb{R}^3$ describes the spatial frequency of the plane wave in the θ and ϕ directions and is given by

$$\mathbf{k} = \begin{bmatrix} k_x \\ k_y \\ k_z \end{bmatrix} = \frac{2\pi}{\lambda} \begin{bmatrix} \sin(\theta)\cos(\phi) \\ \sin(\theta)\sin(\phi) \\ \cos(\theta) \end{bmatrix} = \frac{2\pi}{\lambda}\mathbf{u}, \tag{3}$$

where $\mathbf{u}$ represents the normalized spatial frequency along each cartesian axis.

It has been shown that RF emissions carrying OAM naturally arise from a UCA through linear phase excitation across the array [10]. The phase weight for the mth element corresponding to the ℓth mode are given by

$$w_{m,\ell} = e^{j\frac{2\pi\ell m}{M}} = e^{j\ell\phi_m}, \tag{4}$$

such that

$$g_\ell(t,\theta,\phi) = \sum_{m=0}^{M-1} w_{m,\ell} s_\ell(t) e^{j\mathbf{k}^T\mathbf{p}_m}, \tag{5}$$

where $g_\ell(t,\theta,\phi)$ is the emission carried by the ℓth mode, and $s_\ell(t)$ is fast-time modulation. The OAM modes are mutually orthogonal such that $\langle g_{l_1}(t,\theta,\phi), g_{l_2}(t,\theta,\phi)\rangle_{\theta,\phi} = \delta(\ell_1 - \ell_2)\langle g_{l_1}(t,\theta,\phi), g_{l_2}(t,\theta,\phi)\rangle_{\theta,\phi}$, thus enabling modal parameterization of the emission (and scatterers of sufficient angular extent) in a manner similar to polarimetry [19]. Fig. 1 depicts the beampattern and phase distribution, in u-space, for an 8-element UCA excited with the OAM mode-1 phase weights, which provides circular spatial lobes and a corresponding phase gradient that varies linearly with respect to rotation about the xy plane.

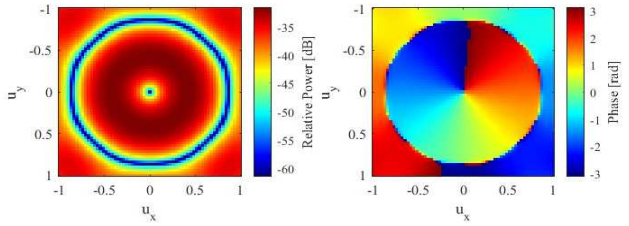

Fig. 1: (left) Beampattern and (right) phase distribution for OAM mode $\ell = 1$, in u-space, implemented on an 8-element UCA.

The representation in (1) denotes the spatial structure of the transmitted field under the assumption of a single time-domain signal. To generalize this model to account for multiple signals, let $s_m(t)$ denote the complex baseband transmit waveform from the mth element. The transmitted field in direction (ϕ,θ) at time t then becomes

$$g(t,\theta,\phi) = \sum_{m=0}^{M-1} w_m s_m(t) e^{j\mathbf{k}^T\mathbf{p}_m}. \tag{6}$$

The general far-field MIMO signal model in (6) permits the transmission of diverse waveforms across the array. This flexibility enables additional design freedom not provided by the element-level weights from (1) in general or the OAM phase weights from (4) specifically.

III. MIMO UCA Signal Processing Description

The transmit and receive channels for a MIMO array can be represented using (6), which captures the full spatial and temporal diversity. Scattering from the environment is modeled via directionally-dependent temporal convolution. Neglecting the individual element gain patterns, the linear model for received data at the l th receive element can therefore be expressed as

$$y_l(t) = \int\int \left\{ \begin{matrix} g(t,\theta,\phi) \\ x(t,\theta,\phi) \end{matrix} * \right\} e^{-j\mathbf{k}^T\mathbf{p}_l}\, d\theta d\phi + n_l(t), \tag{7}$$

where $x(t,\theta,\phi)$ is the spatio-temporal scattering response which incorporates the Jacobian for spherical integration for brevity.

To process the received data, we adopt the method of phase-mode excitation beamforming from [6]. Because the azimuthal angle ϕ and the OAM mode indices are Fourier duals, we transform the received data from element-space into "mode-space", which is accomplished via the linear transformation

$$\tilde{\mathbf{y}}(t) = \mathbf{W}^H\mathbf{y}(t), \tag{8}$$

where $\mathbf{W} \in \mathbb{C}^{M\times 2L-1}$ for $L \le \lfloor M/2 \rfloor$ is the phase-mode transformation matrix with entries $w_{m,\ell} = e^{j\phi_{m,\ell}}$, and $\mathbf{y}(t) = [y_0(t), \dots, y_{M-1}(t)]^T$ is the time-dependent vector of received data channels. Receive beamforming via discrete Fourier transform (DFT) is used to obtain azimuthal signals via

$$\tilde{y}(t,\theta,\phi) = \left(\mathbf{b}(\theta) \odot \mathbf{v}(\phi)\right)^H \tilde{\mathbf{y}}(t), \tag{9}$$

in which $\mathbf{v}(\phi) = \left[e^{-jL\phi}, \dots, e^{j0}, \dots, e^{jL\phi}\right]^T$ is the modal DFT vector converting to azimuth, and the array elevation information is encoded in vector $\mathbf{b}(\theta) = \left[J_{-L}\left(2\pi\frac{R_0}{\lambda}\sin(\theta)\right), \dots, J_L\left(2\pi\frac{R_0}{\lambda}\sin(\theta)\right)\right]$ with $J_\ell(\cdot)$ the ℓ th order Bessel function of the first kind.

For the above model, the signal-to-noise ratio (SNR) maximizing (matched) filter is applied by correlating the modeled transmission at each angle with the received data, which is expressed mathematically as

$$\hat{x}(t,\theta,\phi) = h_{MF}(t,\theta,\phi) * \tilde{y}(t,\theta,\phi) \tag{10}$$

for

$$h_{MF}(t,\theta,\phi) = \frac{\tilde{g}^*(-t,\theta\,\phi)}{\left(\int_0^T |\tilde{g}(t,\theta\,\phi)|^2 dt\right)^{1/2}}. \tag{11}$$

Here $\tilde{g}(t,\theta\,\phi)$ is obtained by expanding the emission via the same phase-mode decomposition as in (8) and (9), i.e.,

$$\tilde{g}(t,\theta\,\phi) = \left(\mathbf{b}(\theta) \odot \mathbf{v}(\phi)\right)^H \mathbf{W}^H\mathbf{s}(t). \tag{12}$$

It should be emphasized that processing with the phase-mode excitation beamformer does not take advantage of the orthogonality of OAM modes. Moreover, the separability between modes only holds for scatterers that are distributed over multiple angular resolution cells. Such an object must also scatter coherently over these resolution cells for the orthogonality between the modes to be leveraged. Consequently, the matched filter response will contain cross-modal interference that sets a floor on estimation performance.

IV. Mapping OAM to High-Power MIMO

To assess emissions that carry multiple OAM modes in a far-field radar context we first wish to pose the signal structure in a

way that can be produced at high-power, meaning a constant-amplitude, spectrally well-contained waveform at each antenna element, which in turn essentially means a MIMO collection of FM signals. This objective motivates a gradient-based optimization framework, whereby the mismatch between the optimized emission and the desired response is measured via the error energy cost function

$$J(\mathbf{s}(t)) = \left\| W\big(G(f,\theta,\phi) - D(f,\theta,\phi)\big)\right\|_2^2, \tag{13}$$

where $G(f,\theta,\phi)$ is the temporal Fourier transform of (6), $D(f,\theta,\phi)$ is the Fourier transform of the ideal far-field emission, and $W(\cdot)$ is the error-weighting function. Ensuring that minimization of (13) provides FM waveforms necessitates constrained optimization, where the constraints are in terms of waveform amplitude

$$|s_m(t)| = c \quad \forall\, t \in (0,T), \tag{14}$$

and spectral containment

$$\|W_c(f) \times S_m(f)\|_2^2 \; < \epsilon \tag{15}$$

for $m \in \{0,\dots,M-1\}$ and a prescribed allowable spectral leakage energy ϵ. In addition to reducing out-of-band spectral content, this latter constraint also serves to limit the per-sample phase-change, which in turn ensures adequate phase continuity when the signal is converted to continuous-time in hardware.

For this work, we are interested in two specific instances of $D(f,\theta,\phi)$. First, consider a scenario where it is desired to generate multi-modal OAM from a single phased array. The desired emission for this case is

$$D_1(f,\theta,\phi) = \sum_{\ell=-L}^{L}\sum_{m=0}^{M-1} D_{1,\ell}(f) w_{m,\ell} e^{j\mathbf{k}^T\mathbf{p}_m}, \tag{16}$$

where $D_{1,\ell}(f)$ is the Fourier transform of (5) accounting for the superposition across OAM modes. Performing this mapping does come at the cost of lost modal isolation since FM waveforms cannot perfectly match (16) because the superposition of concurrent OAM modes would require AM across the array, which is the very attribute we wish to avoid for operation at high-power.

Another emission structure of interest is a more general MIMO case where we relax the specification of imposing specific OAM modes on the emission and instead prescribe a beam of specified width relative to the nominal array resolution for the UCA. This instance has a desired spectrum described by

$$D_2(f,\theta,\phi) = |D_2(\theta,\phi)| e^{j\angle D_2(t,\theta,\phi)}, \tag{17}$$

where $\angle D_2(f,\theta,\phi)$ is a space-frequency phase distribution, and $|D_2(\theta,\phi)|$ is the desired beampattern described by

$$|D_2(\theta,\phi)| = \begin{cases} c, & u_x^2 + u_y^2 \le (\beta_u)^2 \\ 0, & else \end{cases}, \tag{18}$$

where c is a constant scalar describing the desired emission amplitude as a function of space, and β_u is the desired peak-to-null beamwidth in u-space. Like the multi-mode OAM case in (16), the $|D_2(\theta,\phi)|$ term cannot be realized with a physical UCA since a perfectly beam-limited emission would necessitate an infinitely large aperture.

To allow for parameterized optimization, these models must be discretized at a high enough sample rate (relative to 3 dB bandwidth) to capture the spectral roll-off. Each waveform is then represented as an N-length discrete-time vector. Collecting the M waveform-discretized vectors into a matrix yields $\mathbf{S} = [\mathbf{s}_0, \mathbf{s}_1, \dots, \mathbf{s}_{M-1}]$. To simplify (15), we optimize the phase of the discretized forms, such that $\mathbf{s}_m = e^{j\boldsymbol{\Psi}_m}$ is the vector of samples for waveform m, with this "angle modulation" form necessitating some way to limit the piece-wise phase changes that ultimately translates into spectral containment (otherwise it becomes general phase modulation). We likewise discretize the u_x and u_y spatial frequency axes into Q_x and Q_y samples, respectively, such that

$$u_{q_x} = \frac{2q_x - Q_x}{Q_x}, q_x \in \{0,1,\dots,Q_x-1\} \tag{19}$$

and with a similar procedure for u_y. These discretizations are used to construct the steering matrix $\mathbf{V} \in \mathbb{C}^{M\times Q_\theta Q_\phi}$ in which $v_{mq} = e^{j\mathbf{k}^T(u_{q_\theta}, u_{q_\phi})\mathbf{p}_m}$.

With the above discretization, we can state the optimization problem as

$$\mathbf{s}_{\text{opt}}(t) = \underset{\boldsymbol{\Psi}}{\text{argmin}} \|\mathbf{W}_e \odot (\mathbf{ASV} - \mathbf{D})\|_2^2 \tag{20a}$$

such that

$$\|\mathbf{W}_c \odot (\mathbf{AS})\|_2^2 < \epsilon, \tag{20b}$$

where $\mathbf{A} \in \mathbb{C}^{Q_f\times N}$ is a Fourier Transform matrix for $Q_f \ge N$ fast-frequency samples (a DFT matrix with the final $Q_f - N$ columns truncated if frequency oversampling is desired). The matrix $\boldsymbol{\Psi} \in \mathbb{R}^{N\times M}$ is the instantaneous waveform phase providing $\mathbf{S} = e^{j\boldsymbol{\Psi}}$, and $\mathbf{D} \in \mathbb{C}^{Q_f\times Q_\theta Q_\phi}$ is the discretized frequency-domain desired response. The masks $\mathbf{W}_\text{e} \in \mathbb{R}^{Q_f\times Q_\theta Q_\phi}$ and $\mathbf{W}_\text{c} \in \mathbb{R}^{Q_f\times M}$ contain the weights controlling the relative importance of error across joint frequency/angle and spectral containment respectively.

Since it is not possible to remove all spectral leakage described by (20b) for time-limited pulses, (20a) can be efficiently solved as a multi-objective optimization. As such, a Pareto-weighted gradient-descent method is leveraged to solve for a set of constant-amplitude, spectrally contained waveforms that are optimal (in a squared error sense) with respect to desired emission $\mathbf{D}$.

The gradient of the error energy from (20a) becomes

$$\begin{aligned}\nabla_{\boldsymbol{\Psi}} J(\boldsymbol{\Psi}) = \; -2\, Im\Big\{\Big[\Big(\mathbf{A}^*\Big((\mathbf{W}_\text{e}\odot\mathbf{W}_\text{e}) \\ \odot\big(\mathbf{A}^H(\mathbf{SV}-\mathbf{D})\big)^*\Big)\Big)\mathbf{V}^H\Big]\odot\mathbf{S}\Big\},\end{aligned} \tag{21a}$$

for $Im\{\bullet\}$ the imaginary part of the argument, and $J(\boldsymbol{\Psi})$ the objective function (20a). The gradient of constraint (20b) is

$$\nabla_{\boldsymbol{\Psi}} C(\boldsymbol{\Psi}) = \; -2\, Im\big\{\mathbf{S}\odot\big[\mathbf{A}^*\big(\mathbf{W}_\text{c}\odot(\mathbf{A}^T\mathbf{S}^*)\big)\big]\big\}, \tag{21b}$$

where $C(\boldsymbol{\Psi})$ is the spectral containment constraint. The Pareto-weighted cost function is therefore

$$J_{\text{tot}}(\boldsymbol{\Psi};\alpha) = \alpha J(\boldsymbol{\Psi}) + (1-\alpha)C(\boldsymbol{\Psi}), \tag{22}$$

yielding the total gradient

$$\nabla_{\boldsymbol{\Psi}} J_{\text{tot}}(\boldsymbol{\Psi};\alpha) = \alpha\nabla_{\boldsymbol{\Psi}} J(\boldsymbol{\Psi}) + (1-\alpha)\nabla_{\boldsymbol{\Psi}} C(\boldsymbol{\Psi}), \tag{23}$$

from which the ith iterative descent step is provided via

$$\boldsymbol{\Psi}_i = \boldsymbol{\Psi}_{i-1} - \mu_i \, \boldsymbol{\nabla}_{\boldsymbol{\Psi}} J_{\text{tot}}(\boldsymbol{\Psi}_{i-1}; \alpha). \tag{24}$$

Here, μ_i is an adaptive step-length parameter implemented via a backtracking line search based on the first Wolfe condition (sufficient cost decrease). In addition, a step growth parameter is employed at each descent iteration to prevent μ_i from prematurely converging to zero [20]. Note that the goal of this optimization is not to design some radar-specific OAM emission. The point here is to determine a mapping from a given idealized emission structure to MIMO FM waveforms, providing a reasonably good solution that permits experimental evaluation in a manner that is sufficiently representative of high-power operation.

V. Simulated Comparison

A comparison is drawn between the two different desired responses discussed in Section IV, when used for UCA MIMO waveform optimization. In the first, a beam is optimized to match a superposition of OAM modes $\ell = \{-1, 0, 1\}$ as described by (16). This scenario is termed the OAM-optimized case and allows us to evaluate the beampattern characteristics of multi-modal OAM. Additionally, it acts as a control scenario against which we may compare more general MIMO emissions in the UCA context. For comparison, we also optimize an array of waveforms to provide a near-identical 3-dB beamwidth to the OAM-optimized emission (roughly 1.5 times the Fourier 3-dB resolution of the array), via (17) and (18). This second scenario is termed the beamwidth-optimized case and allows us to examine the tendency of general MIMO emissions from a UCA to intrinsically carry dynamic weightings of OAM modes.

For the simulation, each waveform has a pulse width of $T = 1\mu s$ and 3-dB bandwidth of $B = 100\ MHz$, and is oversampled in time by $K_{\text{os}} = 4$. In each case, 3000 Monte Carlo realizations are randomly initialized across the cost surface, with each optimized for 100 iterations, which has been observed to ensure convergence among all realizations. The waveforms are simulated for an 8-element UCA ($M = 8$) with inter-element spacing $d = 0.55\lambda$ (a spacing chosen to match the physical array used for open-air experiments).

The fast-frequency content of each mode in the OAM-optimized desired response, denoted $D_{1,\ell}(f)$ in (16), is chosen to be a separately generated pseudo-random optimized FM (PRO-FM) waveform [21], which provides strict spectral containment. For the array of beamwidth-optimized waveforms, the magnitude of the desired response is chosen to be a constant value within a circle of 1.5 times radius of the UCA's half-power beamwidth, and the phase is derived from a modeled emission of uncorrelated PRO-FM waveforms transmitted from each element.

Fig. 2 illustrates the desired versus optimized beampatterns and phase distributions for a single initialization of the OAM-optimized cases. The optimized patterns closely match the desired multi-modal OAM field, especially in areas where the desired power is high, which results in a higher cost when a uniform error weighting is chosen.

The beamwidth-optimized realization is depicted in Fig. 3. Specifically, Fig.3b shows that the beamwidth-optimized case results in a near-constant power distribution across the main beam, resulting from the desired power pattern in Fig. 3a. The optimized phase distribution in Fig. 3d closely aligns with the desired pattern in Fig. 3c, preserving the spatial phase progression imposed by the PRO-FM waveform initializations.

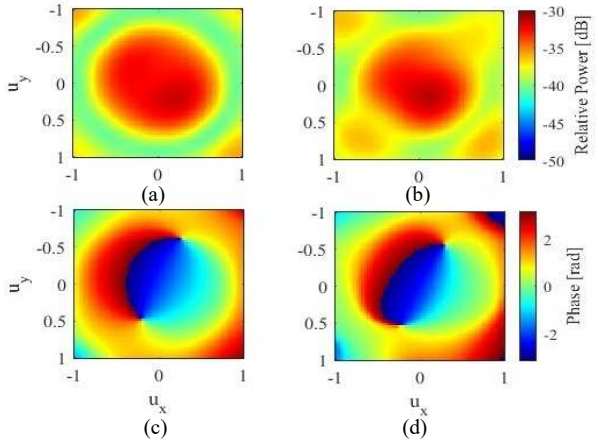

Fig. 2: OAM-optimized simulated emission for (a) the desired beampattern, (b) the optimized beampattern, (c) the desired phase pattern, and (d) the optimized phase pattern.

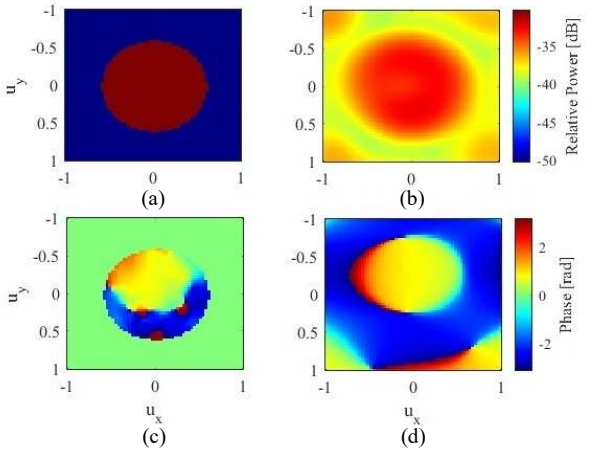

Fig. 3: Beamwidth-optimized simulated emission for (a) the desired beampattern, (b) the optimized beampattern, (c) the desired phase pattern, and (d) the optimized phase pattern.

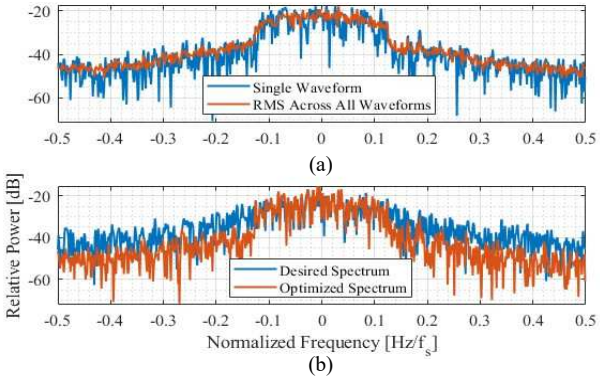

Fig. 4: Beamwidth-optimized spectra for (a) a single waveform compared to the RMS average across all waveforms, and (b) the desired emission vs. the optimized emission.

Representative power spectra for the beamwidth-optimized case, are shown in Fig. 4 (the OAM-optimized case is omitted

since it produces nearly identical results). Fig. 4a depicts the spectra for the individual waveforms compared to their root mean-square (RMS), showing that the optimization results in spectrally-contained waveforms. Fig. 4b depicts the fast-time spectrum of the far-field emissions at the peak-gain spatial direction, which shows that the optimized emission closely matches the desired response within the passband.

To evaluate the mapping between the idealized desired responses and the optimized emissions, a series of metrics were computed for the Monte Carlo trials, with the primary metrics being emission match error from (13) and the spectral leakage energy from (20b). Since the emission is being generated through FM waveforms, the desired OAM modes will not be excited in isolation, but in conjunction with all other possible modes. As such, another quantity of interest is the optimized contribution from each excited phase mode $\eta_\ell(t)$ given by

$$\eta_\ell(t) = \frac{\mathbf{s}^H(t)\mathbf{w}_\ell}{\|\mathbf{s}(t)\|_2\|\mathbf{w}_\ell\|_2}. \tag{25}$$

Computing $\eta_\ell(t)$ for a specific Monte Carlo realization of the beamwidth-optimized case results in Fig. 5. For the emission to achieve the desired beamspoiling, the contribution of each mode must change dynamically over the pulse. It should be noted that near-identical results were observed for the OAM-optimized case.

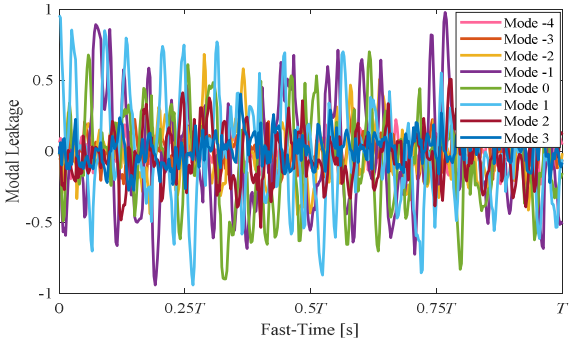

Fig. 5: Modal leakage across time for the beamwidth-optimized emission.

By taking the RMS average across the temporal content of $\eta_\ell(t)$, we can compute the average contribution of each mode, which is depicted in Fig. 6. This result shows that the OAM-optimized case successfully compresses much of its energy evenly into modes{-1, 0, 1}, while the beamwidth-optimized case relies more heavily on modes -1 and 1 to achieve the desired spatial coverage. Despite these small differences, Fig. 6 shows that UCA MIMO emissions of similar beamwidths tend to prioritize similar OAM modes, even when OAM attributes are not an explicit part of the design.

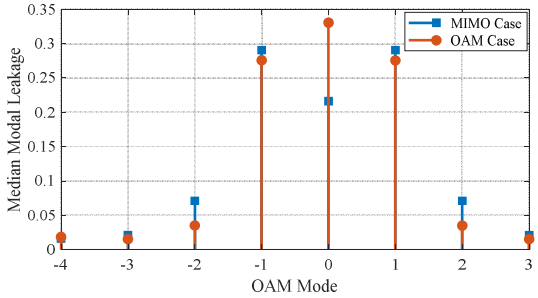

Fig. 6: Median modal leakage across Monte Carlo trials for beamwidth-optimized and OAM-optimized emissions.

The final metric is the peak spatial gain provided by the energy-normalized emission, which is computed by

$$|g_{peak}|^2 = \frac{\max\limits_{\theta,\phi}\left\{\text{rms}\{g(t,\theta,\phi)\}\right\}}{\|g(t,\theta,\phi)\|_2^2} \tag{26}$$

and provides a measure of the array's focusing capability for the two optimized emissions. Since inclusion of higher order modes implies a broader energy spread across u_x and u_y, it can be inferred that (26) should be lower for emissions containing significant energy in higher modes.

The statistical results obtained from Monte Carlo simulations are depicted in Table I. These results indicate that both the OAM-optimized and beamwidth-optimized cases achieve similar match errors and out-of-band spectral leakage, though the OAM-optimized case does provide slightly better values on average. The discrepancy here can be attributed to the ease with which the array can match the phase content of each desired response. The peak spatial gain shows a similar trend, with the OAM-optimized case being 0.9 dB higher across the ensemble, though with a less even distribution of energy across the mainlobe. The values for the modal contributions are listed for the positive modes only since the negative modes were approximately symmetric (per Fig. 4). As expected, the strongest modal contribution for both cases occurs for the modes specifically included in the OAM-optimized emission. Of course, it is interesting to note that the beamwidth-optimized case yields similar modal contributions despite the lack of OAM design attributes, which can be attributed to an emergent phenomenon of UCAs.

Table 1: Performance Metrics from Monte Carlo

Metrics		**OAM-optimized**		**Beamwidth-optimized**	
		Median	Std. Dev.	Median	Std. Dev.
$J(\mathbf{\Psi})$		-6.83dB	-44.97dB	-1.38dB	-41.33dB
$C(\mathbf{\Psi})$		-12.22dB	-32.99dB	-12.87dB	-33.70dB
Δ_{peak}		-31.60dB	-64.25dB	-32.5dB	-66.07dB
Modal Contribution $\eta(\ell)$	0	0.331	0.008	0.216	0.018
	-1	0.275	0.005	0.291	0.029
	-2	0.035	0.002	0.071	0.007
	-3	0.015	0.001	0.021	0.002
	-4	0.018	0.001	0.016	0.001

VI. Open-Air Experimentation

To experimentally examine the sensing capabilities of the UCA MIMO emissions, an open-air experiment was conducted using the Waveform Diversity Experimentation System (WaDES), which is an X-band MIMO radar testbed at the University of Kansas. For this experiment, both the transmitter and receiver were fitted with 8-element UCAs having an inter-element spacing of 0.55λ. The transmission consisted of 100 pulses, centered at 8.75 GHz with a pulsewidth of $T = 1\ \mu$s and bandwidth $B = 100$ MHz. The pseudo-monostatic experimental setup is shown in Fig. 7, depicting the receiver placed roughly 8 m behind the transmitter to mitigate direct-path coupling. The scatterer of interest for this test is the Salina Piece, a large metal sculpture located at 107 m range, $-60°$ in azimuth, and $+10°$ in elevation with respect to the transmitter.

Fig. 7: Experimental setup: the left rack is the WaDES receiver and the right rack is the WaDES transmitter. The Salina Piece is circled in red.

Using the matched-filtering framework described in Sect. III, the beamwidth-optimized receive data was compressed to obtain range and spatial estimates of the scene, with results provided in Figs. 8 and 9. The received response is beamformed in the direction of the Salina Piece and the resulting range profile of the scene is shown in Fig. 8. Additionally, Fig. 9 displays the spatial response extracted from the 107 m range bin containing the scattering of interest. This spatial spectrum corresponding to the Salina Piece depicts a visible peak at the correct azimuth and elevation, with an additional conjugate symmetric response as a result of the full rotational symmetry of the UCA [6].

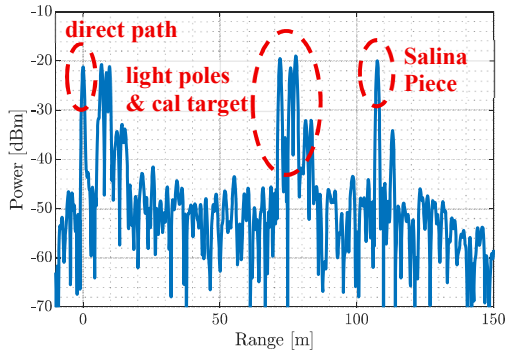

Fig. 8: Range profile beamformed towards the Salina Piece.

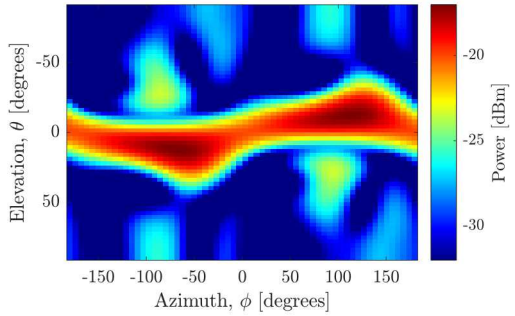

Fig. 9: Spatial response at R = 107 m depicting symmetric returns from Salina Piece.

VI. Conclusions

The generation of physical MIMO radar emissions from a UCA has been examined, recognizing OAM as an emergent property of EM waves transmitted from circular apertures. To ensure high-power applicability, optimization was performed to realize FM waveforms in a MIMO radar context. The resulting waveforms were used to generate spatially-diverse emissions that were evaluated via Monte Carlo simulation and open-air experimentation. The results display OAM characteristics even when such considerations were not included in the design framework, illustrating that OAM modes act as a natural basis for emissions transmitted from circular arrays.

References

[1] N.H. Lehmann, A.M. Haimovich, R.S. Blum, L. Cimini, "High resolution capabilities of MIMO radar," *Asilomar Conf. Signals, Systems & Computers*, Pacific Grove, CA, Oct. 2006.

[2] G. Zook, P. McCormick, S.D. Blunt, "Fixational eye movement radar: random spatial modulation," *IEEE Radar Conf.*, Oklahoma City, OK, Apr. 2018.

[3] D.R. Fuhrmann, G. San Antonio, "Transmit beamforming for MIMO radar systems using signal cross-correlation," *IEEE Trans. Aerospace & Electronic Systems*, vol. 44, no. 1, pp. 171-186, Jan. 2008.

[4] P. Stoica, J. Li, Y. Xie, "On probing signal design for MIMO radar," *IEEE Trans. Signal Processing*, vol. 55, no. 8, pp. 4151-4161, Aug. 2007.

[5] M.B. Heintzelman, D.B. Herr, C.A. Mohr, S.D. Blunt, C. Sahin, A. Kordik, "Separability analysis of random FM radar waveforms," *IEEE Trans. Radar Systems*, vol. 3, pp. 768-788, May 2025.

[6] H.L. Van Trees, *Optimum Array Processing*. New York, NY, Wiley, 2002.

[7] A. Veneri, P. Burghignoli, D. Comite, "Microwave imaging with circular arrays: comparative analysis between OAM and MIMO," *IEEE Trans. Antennas & Propagation*, vol. 73, no. 5, pp. 3015-3025, May 2025.

[8] L. Allen, M.W. Beijersbergen, R.J.C. Spreeuw, J.P. Woerdman, "Orbital angular momentum of light and the transformation of Laguerre-Gauss laser modes," *Phys. Rev. A*, vol. 45, no. 11, pp. 8185–8189, Jun. 1992.

[9] G. Gibson, J. Courtial, M.J. Padgett, M. Vasnetsov, V. Pas'ko, S.M. Barnett, S. Franke-Arnold, "Free-space information transfer using light beams carrying orbital angular momentum," *Opt. Express*, vol. 12, no. 25, pp. 5448–5456, Nov. 2004.

[10] B. Thidé, H. Then, J. Sjöholm, K. Palmer, J. Bergman, T.D. Carozzi, Y.N. Istomin, N.H. Ibragimov, R. Khamitova, "Utilization of photon orbital angular momentum in the low-frequency radio domain," *Phys. Rev. Lett.*, vol. 99, no. 8, Aug. 2007.

[11] S.M. Mohammadi, et al., "Orbital angular momentum in radio—a system study," *IEEE Trans. Antennas & Propagation*, vol. 58, no. 2, pp. 565-572, Feb. 2010.

[12] K. Liu, Y. Cheng, Z. Yang, H. Wang, Y. Qin, X. Li, "Orbital-angular-momentum-based electromagnetic vortex imaging," *IEEE Antennas & Wireless Propagation Letters*, vol. 14, pp. 711-714, Sept. 2015.

[13] R. Chen, H. Zhou, M. Moretti, X. Wang, J. Li, "Orbital angular momentum waves: generation, detection, and emerging applications," *IEEE Communications Surveys & Tutorials*, vol. 22, no. 2, pp. 840-868, Second quarter 2020.

[14] F. Tamburini, E. Mari, A. Sponselli, B. Thide, A. Bianchini, F. Romanato, "Encoding many channels on the same frequency through radio vorticity: first experimental test," *New Journal of Physics,* vol. 14, no. 3, pp. 1-17, Mar. 2012.

[15] K. Liu, et al., "Generation of OAM beams using phased array in the microwave band," *IEEE Trans. Antennas & Propagation*, vol. 64, no. 9, pp. 3850-3857, Sept. 2016.

[16] Q. Bai, A. Tennant, B. Allen, M.U. Rehman, "Generation of orbital angular momentum (OAM) radio beams with phased patch array," Loughborough Antennas & Propagation Conference, Loughborough, Eng, Nov. 2013.

[17] W. Lv, K.J. Mishra, J. Hu, "Twisting signals for joint radar-communications: an OAM vortex beam approach," 10.48550/arXiv.2509.15601.

[18] F. Tamburini, B. Thide, E. Mari, A. Sponselli, A. Bianchini, F. Romanato, "Reply to comment on 'encoding many channels on the same frequency through radio vorticity: first experimental test'," *New Journal of Physics*, vol. 14, no. 11, p. 118002, Nov. 2012.

[19] P. McCormick, J. Jakabosky, S.D. Blunt, C. Allen, B. Himed, "Joint polarization/waveform design and adaptive receive processing," *IEEE Intl. Radar Conf.*, Arlington, VA, May 2015.

[20] C.A. Mohr, P.M. McCormick, C.A. Topliff, S.D. Blunt, J.M. Baden, "Gradient-based optimization of PCFM radar waveforms," *IEEE Trans. Aerospace & Electronic Systems*, vol. 57, no. 2, pp. 935-956, Apr. 2021.

[21] J. Jakabosky, S.D. Blunt, B. Himed, "Spectral-shape optimized FM noise radar for pulse agility," *IEEE Radar Conf.*, Philadelphia, PA, May 2016.

[22] Li, Z., Qu, F., Wei, Y. *et al.* The Limits of Effective Degrees of Freedom in UCA based Orbital Angular Momentum Multiplexed Communications. *Sci Rep* **10**, 5216 (2020).